

Combining an *in silico* proarrhythmic risk assay with a tPKPD model to predict QTc interval prolongation in the anesthetized guinea pig assay

Pierre Morissette^{a,*}, Sebastian Polak^{b,f}, Anne Chain^c, Jin Zhai^a, John P. Imredy^a, Mary Jo Wildey^d, Jeffrey Travis^a, Kevin Fitzgerald^a, Patrick Fanelli^a, Elisa Passini^e, Blanca Rodriguez^e, Frederick Sannajust^a, Christopher Regan^a

^a Safety Assessment & Laboratory Animal Resources (SALAR), Merck & Co., Inc., West Point, PA, USA

^b Certara UK Limited, Simcyp Division, Sheffield, UK

^c Pharmacokinetics, Pharmacodynamics and Drug Metabolism (PPDM), Merck & Co., Inc., Rahway, NJ, USA

^d Pharmacology, Screening and Informatics, Merck & Co., Kenilworth, NJ, USA

^e Computational Cardiovascular Science Group, Department of Computer Science, BHF Centre of Research Excellence, University of Oxford, Oxford, UK

^f Jagiellonian University Medical College, Faculty of Pharmacy, Krakow, Poland

ARTICLE INFO

Keywords:

Anesthetized Cardiovascular Guinea Pig
In Silico modeling
 QT corrected interval
 Torsade de Pointes
 Translational PKPD modeling
 Safety pharmacology

ABSTRACT

Human-based *in silico* models are emerging as important tools to study the effects of integrating inward and outward ion channel currents to predict clinical proarrhythmic risk. The aims of this study were 2-fold: 1) Evaluate the capacity of an *in silico* model to predict QTc interval prolongation in the *in vivo* anesthetized cardiovascular guinea pig (CVGP) assay for new chemical entities (NCEs) and; 2) Determine if a translational pharmacokinetic/pharmacodynamic (tPKPD) model can improve the predictive capacity. *In silico* simulations for NCEs were performed using a population of human ventricular action potential (AP) models. PatchXpress® (PX) or high throughput screening (HTS) ion channel data from respectively $n = 73$ and $n = 51$ NCEs were used as inputs for the *in silico* population. These NCEs were also tested in the CVGP ($n = 73$). An M5 pruned decision tree-based regression tPKPD model was used to evaluate the concentration at which an NCE is liable to prolong the QTc interval in the CVGP. *In silico* results successfully predicted the QTc interval prolongation outcome observed in the CVGP with an accuracy/specificity of 85%/73% and 75%/77%, when using PX and HTS ion channel data, respectively. Considering the tPKPD predicted concentration resulting in QTc prolongation (EC₅₀) increased accuracy/specificity to 97%/95% using PX and 88%/97% when using HTS. Our results support that human-based *in silico* simulations in combination with tPKPD modeling can provide correlative results with a commonly used early *in vivo* safety assay, suggesting a path toward more rapid NCE assessment with reduced resources, cycle time, and animal use.

1. Introduction

Drug-induced cardiac proarrhythmic risk, including polymorphic ventricular tachycardic arrhythmias and, in particular, Torsade de Pointes (TdP), represents a life-threatening adverse effect. They have not only led to the withdrawal of marketed products (Heist and Ruskin,

2010), but the risk of such events continues to be a significant reason for drug development attrition. This resulted in the creation of two important documents by the International Conference on Harmonization of Technical Requirements for Registration of Pharmaceuticals for Human Use (ICH): 1) the preclinical ICH-S7B guideline describing the preclinical evaluation of cardiac proarrhythmic risk and 2) the E14

Abbreviations: AP, Action Potential; APD₉₀, Action Potential Duration at 90% repolarization; BP, Blood Pressure; CVGP, Cardiovascular Anesthetized Guinea Pig; CTD₉₀, Ca²⁺-Transient Duration at 90% repolarization; ECG, Electrocardiogram; EMw, Electromechanical window; FIH, First in Human; FLIPR, Fluorescent Imaging Plate Reader; FN, False Negative; FP, False Positive; GP, Guinea Pig; hERG, Human Ether-a-go-go Related Gene; HR, Heart Rate; HTS, High Throughput Screening; ICH, The International Council for Harmonization of Technical Requirements for Pharmaceuticals for Human Use; I_{Kr}, rapidly-activating delayed rectifier potassium current; LOO, Leave-One-Out; LVP, Left Ventricular Pressure; M5P, M5 trees automated pruning model; NCEs, New Chemical Entities; ORd, O'Hara Rudy model; PNV, Predictive Negative Value; PPV, Positive Predictive Value; PX, PatchXpress®; QTc, Heart Rate corrected QT Interval; QTcVdW, Van de Water's Heart Rate QT-corrected Interval; TdP, Torsade de Pointes; tPKPD, translational pharmacokinetic/pharmacodynamic; TN, True Negative; TP, True Positive

* Corresponding author at: Safety Assessment & Laboratory Animal Resources, Merck & Co. Inc., 770 Sumneytown Pike, PO. Box 4, West Point, PA 19486, USA.

E-mail address: pierre_morissette@merck.com (P. Morissette).

<https://doi.org/10.1016/j.taap.2020.114883>

Received 11 September 2019; Received in revised form 3 January 2020; Accepted 14 January 2020

Available online 23 January 2020

0041-008X/ © 2020 The Authors. Published by Elsevier Inc. This is an open access article under the CC BY license

(<http://creativecommons.org/licenses/by/4.0/>).

guideline discussing the evaluation of proarrhythmic risk in humans. The S7B guideline recommended the evaluation of new drug candidates for effects on I_{Kr} or Human Ether-a-go-go Related Gene (hERG) *in vitro* and on the QTc interval *in vivo* as primary preclinical studies to evaluate their potential for drug-induced QTc interval prolongation and arrhythmogenesis. Although these ICH guidelines were in response to a critical health concern, their reliance solely on hERG inhibition and/or QTc interval prolongation may have limited the advancement of potentially safe and effective drugs that caused QTc interval prolongation but with no or acceptable arrhythmogenic potential to market (Salvi et al., 2010).

It is widely accepted that the major cellular mechanism enabling TdP is the blockade of the rapidly activating delayed rectifier potassium current (I_{Kr}), encoded by *hERG* (or *KCNH2*). However, it has been well documented that: 1) hERG inhibition on its own does not always translate to the occurrence of TdP, 2) action potential duration (APD) prolongation *in vitro* is not always associated with the clinical prolongation of the QTc interval and, 3) a prolonged QTc interval does not always linearly correlate to the occurrence of TdP. The generally accepted explanation for these discrepancies is that although the inhibition of I_{Kr} plays a critical role in delaying repolarization, activation of inward late sodium (late I_{Na}) and/or calcium currents (I_{Ca}) have been shown to be needed to generate a proarrhythmic response (Nemec et al., 2016). As such, drugs that inhibit both inward (late I_{Na} and I_{Ca}) and outward (I_K) cardiac currents (e.g. ranolazine, verapamil) tend to prolong the QTc interval, but are not associated with the generation of TdP due to the blockade of inward currents (Fermini and Fossa, 2003; Fermini et al., 1995).

As a result, evaluation of cardiac proarrhythmic risk during drug development is evolving. The new emphasis is placed on assessing comprehensive drug-induced proarrhythmic risk rather than the traditional assessment of preclinical hERG blockade-related QTc interval prolongation. To that extent, “the comprehensive *in vitro* proarrhythmia assay” (CiPA) was established to develop a new paradigm for assessing proarrhythmic risk. One of the pillars of this initiative includes *in silico* integration of cellular electrophysiologic effects based on ionic current effects. *In silico* assays have a great potential to provide an integrative assessment of mixed cardiac ion channel inhibition as well as a high-throughput (HTS) assessment of proarrhythmic risk in early drug development. *In silico* modeling and simulation is beginning to be utilized more frequently to predict clinical proarrhythmic risk and also the outcome of preclinical *in vivo* or *ex vivo* models that generally are conducted later in drug development (Passini et al., 2017). Previous studies have evaluated the ability of *in silico* assays to predict the outcome of more resource intensive *in vivo* models such as drug effects on APD in isolated canine cardiomyocytes and in the rabbit ventricular wedge, respectively (Beattie et al., 2013; Davies et al., 2012).

Our current approach is analogous as it evaluates *in silico* simulations of action potential duration and electromechanical window (EMw) results (Morissette et al., 2016; Passini et al., 2019) to predict the QTc interval results in the cardiovascular anesthetized guinea pig assay (Morissette et al., 2013). Furthermore, this study also evaluates the usefulness of combining a mathematical translational pharmacokinetic/pharmacodynamic (tPKPD) model with the *in silico* qualitative endpoints to better predict the CVGP results. This tPKPD relationship could enable the prediction of unbound plasma concentration at which a new chemical entity (NCE) presents a QTc interval prolongation risk in the anesthetized CVGP assay. In turn, simulations using combined *in silico* and tPKPD models could help identify potential pro-arrhythmic agents and determine the relevant concentration at which they may have a meaningful effect in animals or humans.

2. Methods

2.1. Statement on use and care of animals

All aspects of the animal use were in accordance with the Guide for the Care and Use of Laboratory Animals (Institute of Laboratory Animal Resources, Commission on Life Sciences, National Research Council, 2011) and approved by the Institutional Animal Care and Use Committee (IACUC) of Merck & Co., Inc., Kenilworth, NJ, USA.

2.2. PatchXpress® (PX) electrophysiology

2.2.1. Measurement of I_{Kr} and I_{Ks} ion channel current activities: PatchXpress® automated patch clamp

Experimental procedures for measurement of I_{Kr} and I_{Ks} with PatchXpress® (PX) were previously described in detail (Trepakova et al., 2007; Zeng et al., 2008). In summary, whole-cell hERG or I_{Ks} currents were measured from heterologous human embryonic cells stably expressing hERG or I_{Ks} (KCNQ1/ KCNE1) channels using the automated PX system, PatchXpress® 7000A (Molecular Devices), at ambient temperature. Resistance of the planar patch plate chambers (SealChip₁₆[™] [AVIVA]) were between 1 and 3 MΩ. For measurement of hERG and I_{Ks} , currents were elicited with their respective voltage-step protocol at 20-s inter-pulse intervals during control conditions and after addition of test compounds. The hERG current was elicited with the following voltage-step protocol: from a holding potential (V_h) of -80 mV, a brief 20-ms depolarizing prepulse to -50 mV was applied to obtain a baseline current followed by a return to V_h for 80 ms, an activating 4-s depolarizing step to a test potential (V_t) of $+20$ mV and a 4-s repolarizing step (repolarizing potential for deactivating tail current [V_{tail}]) to -50 mV.

The KvLQT1/KCNE1 current (I_{Ks}) was elicited from a V_h of -50 mV with 3-s depolarizing steps to a V_t of $+50$ mV then followed by a 3-s repolarizing step (V_{tail}) to -50 mV. Both hERG and I_{Ks} currents were quantified as peak deactivating tail current amplitude during V_{tail} . Currents were monitored for stability for 5-min period before addition of the vehicle alone (DMSO control) or test agents diluted from stocks in 10 mM DMSO. Test agents were applied (60 μ l) at sequentially increasing concentrations at a rate of 25 μ l/s. For each condition or drug concentration, duplicate or triplicate 60 μ l additions were made to each test well at 11-s intervals in order to achieve equilibrium and current was monitored for 5-min period at each condition or test agent concentration.

2.2.2. I_{Na} channel activity measurements: PatchXpress automated patch clamp

A human cell line stably expressing the hNav1.5, the electrophysiological recording solutions and the methods for the determination of activity on the cardiac Na^+ channel were described previously (Penniman et al., 2010).

Briefly, whole cell hNav1.5 currents (I_{Na}) were recorded from isolated HEK-293 cells using 16-chamber planar glass electrodes (Sealchip[™]) and the whole-cell variant of the PX technique with the PatchXpress® 7000A automated PX (Molecular Devices, Sunnyvale, CA). SealChip ‘hole’ resistances were between 1 MΩ and 3 MΩ in the presence of the indicated recording solutions. Whole-cell hNav1.5 currents were low-pass filtered at a cut-off frequency of 3 kHz and digitally sampled at 15 kHz. hNav1.5 current was elicited using 30-ms pulses to -20 mV from a V_h of -100 mV and quantified using the amplitude of the negative (inward) peak current. Following vehicle or test article addition, voltage pulses were applied at a rate of 0.2 Hz for at least 6 min to allow equilibration of the current to a new steady state. Subsequently, a train of 60 pulses was applied at a rate of 3 Hz to determine rate-dependent effects of the test article. Typically, three ascending test article concentrations were tested sequentially in half-log increments on each cell. For each condition, i.e., a given pulsing rate

and test concentration, peak inward Na^+ current amplitudes were quantified as the average of final three pulses in a train.

2.3. Measurement of MK-499 binding, I_{CaL} and I_{Na} channel activity by high throughput screening (HTS) methods

2.3.1. MK-499 filter binding assay

This method is an *in vitro* test for the inhibition of ^{35}S -MK-499 binding to the hERG channel expressed in HEK293 cells, known as hERG-1B/HEK293 cell line.

Cell membranes were prepared from HEK-293 cells constitutively expressing hERG. Cells were harvested and homogenized in Tris-EDTA buffer containing 50 mM Tris and 1 mM EDTA, pH 7.4. Homogenates were centrifuged at 45,000g for 50 min at 4 °C. The pellet was washed once in Tris-EDTA, centrifuged, resuspended at a concentration of 5 mg/ml in binding buffer containing (in mM) 70 NaCl, 60 KCl, 1 CaCl_2 , 2 MgCl_2 , and 10 HEPES, pH 7.4, and stored at -70 °C.

On the day of the assay, hERG membranes were thawed and diluted to a concentration of 180 $\mu\text{g}/\text{ml}$ in binding buffer and 25 μL of membrane were added to each well of a 384 W deep well block (Axygen, P-384-120SQ-C). For competition binding studies, 1 μL of test compounds in DMSO at varying concentrations or DMSO alone (control) were added to the wells containing membrane. The binding reaction was initiated by adding 25 μL of ^{35}S -labeled MK-499 (750–850 Ci/mmol, custom synthesis, Perkin Elmer) was added (achieving a final concentration of 50 pM). After incubation for 90 min at room temperature, the binding was stopped by filtration of membranes through a 384-well Multiscreen-HTS FC filter plate (Millipore, MZFCNOW50) that was prewet before filtration with 20 μL of prewet buffer (0.01% Poly (ethyleneimine) (Sigma, P3143), 0.01% Triton X-100 (SigmaUltra, T9284)). The filters were washed using a Biotek Elx405 plate washer that has been primed with cold 1 \times wash buffer (20 \times Wash Buffer: 1 M HEPES/NaOH, pH 7.4, 200 ml; 5 M NaCl, 520 mL; 1 M MgCl_2 , 40 mL; 1 M CaCl_2 , 20 mL; DH20, 220 mL). The assay mixture is transferred to the filter plate and then each assay plate well is washed with 30 μL /well of room temperature 1 \times wash buffer to ensure the assay mixture is completely removed. The filter plate was washed with 1 \times cold wash buffer with 100 μL /well, twice. Washed filter plates were dried for at least 75 min in a 55 °C oven, and radioactivity associated with each filter was measured by the addition of 10 μL Microscint-0 (Perkin Elmer 6,013,611) scintillation liquid and counting in a 384-well scintillation counter (Topcount or MicroBeta, Perkin Elmer).

2.3.2. Ca^{2+} influx fluorescence (FLIPR) assay

Human L-type calcium channels (hCav1.2) composed of 3 calcium channel subunits (α_{1C} , $\alpha_{2\delta}$, β_{2a}) (Balasubramanian et al., 2009) were stably expressed in HEK-293 cells, along with an inwardly-rectifying potassium channel, hKir_{2.3}, to set a more negative resting membrane potential (-65 mV at an external K^+ concentration, $[\text{K}^+]_o$, of 5.8 mM) and promote depolarization of the resting membrane potential by raising $[\text{K}^+]_o$ (Xia et al., 2004) and thereby increasing the K^+ equilibrium potential. HEK-293 cells were grown in culture media containing DMEM (Gibco 11,960), without glutamine and sodium pyruvate, but with 4.5 g/L D-Glucose; supplemented with 10% fetal bovine serum, 100 U/ml penicillin, and 100 $\mu\text{g}/\text{ml}$ streptomycin, as well as selection antibiotics Geneticin G418 (100–800 $\mu\text{g}/\text{ml}$) for α_{1C} , Zeocin (40 $\mu\text{g}/\text{ml}$) for Kir2.3, and Hygromycin B (100–250 $\mu\text{g}/\text{ml}$) for β_{2a} . HEK-Cav1.2 cells were incubated at 37 °C in filtered ambient air supplemented with 5% CO_2 . Cells were grown to approximately 70–80% confluency and passaged twice-a-week. All tissue culture reagents were obtained from ThermoFisher Scientific/LifeTechnologies.

Prior to conducting assays, cells were seeded in poly-D-lysine coated 384-well plates (BioCoat) at 60 K cells per well and incubated for ≤ 24 h at 37 °C. On the day of assay conduct, cells were rinsed with wash buffer (containing in mM: 5.8 KCl, 146.2 NaCl, 0.005 CaCl_2 , 1.7 MgCl_2 , and 10 HEPES) and then incubated in wash buffer supplemented

with 4 μM FLUO-4 AM, 0.02% Pluronic acid (both from Molecular Probes), and 10 mM D-glucose for 30 min at room temperature in the dark. After this Ca^{2+} -sensitive dye loading step, cells were washed with and then kept in 0.05 ml incubation buffer (containing in mM: 25 KCl, 127 NaCl, 0.005 CaCl_2 , 1.7 MgCl_2 , and 10 HEPES) with test agent or positive or negative control drugs at various test concentrations for 30 min at room temperature in the dark. All buffers were adjusted to pH 7.5 with NaOH or HCL prior to use. The plate was subsequently placed in the reading chamber of a fluorimeter (FLIPR^{TETRA}, Molecular Devices) and the emission of each well at a wavelength of 535 nm was measured in response to excitation at a wavelength 480 nm at sampling intervals of 1.6 s.

Following a baseline reading for 10–20 s, Ca^{2+} -trigger buffer (containing in mM: 119 NaCl; 25 KCl; 4 mM CaCl_2 ; 1.7 MgCl_2 and 10 HEPES) was added at a volume equal to that of the incubation buffer already present in the well, after which the emission intensity at 535 nm was measured for another 20–30 s. The Ca^{2+} influx signal was quantified as the difference between the baseline and the peak of the emission signal in response to the addition of Ca^{2+} -trigger buffer, which was typically reached within 20 s thereafter. The Ca^{2+} signal from each well containing test agent was normalized to a signal window defined as the difference between the positive (100% inhibition) and negative (0% inhibition) control signals.

2.3.3. hNav1.5 FLIPR assay

The HEK-hNav1.5 cell line is a stably transfected HEK-293 cell line over expressing hNav1.5. Cells were grown in culture media containing MEM (Gibco 3230–026), supplemented with 10% fetal bovine serum (Hyclone SH30070.02), 1% penicillin/streptomycin/L-Glutamine (Gibco 10,378–016), 1% non-essential amino acids (Gibco 11140-035). HEK-hNav1.5 cells were incubated at 37 °C with 5% CO_2 . Cells were grown to approximately 70–80% confluency and passaged twice a week.

Prior to conducting assays, cells were seeded in poly-D-lysine coated 384-well plates (BD Biosciences 356,697) at 15 K cells per well and incubated for 48 h at 37 °C.

On the day of assay, cells were washed with assay buffer (containing in mM: 4.5 KCl, 165 NaCl, 2 CaCl_2 , 1 MgCl_2 , 10 glucose, and 10 HEPES) and then incubated in 25 μL 1 \times blue dye solution (Molecular Devices BLUE R8042 diluted in assay buffer). Test agent or positive or negative control drugs at various test concentrations were added and incubated for a 30-min period at room temperature in the dark. The plate was subsequently placed in the reading chamber of a fluorimeter (FLIPR^{TETRA}, Molecular Devices) and the emission of each well at a wavelength of 565 nm was measured in response to excitation at a wavelength 510 nm at sampling intervals of 3.5 s for 60 reads. Following a baseline read, 25 μL of 60 μM veratridine (Sigma-Aldrich V5754–25 MG) prepared in assay buffer was added, after which the emission intensity at 565 nm was measured for another 60 reads. The signal was quantified as the difference between the baseline and the peak of the emission signal in response to the addition of Veratridine, which was typically reached within 20 s thereafter. The Ca^{2+} signal from each well containing test agent was normalized to a signal window defined as the difference between the positive (100% inhibition) and negative (0% inhibition) control signals.

2.4. Anesthetized Guinea pig assay

Details of the anesthetized CVGP assay have been described previously in Morissette et al. (2016). Briefly, male Hartley guinea pigs (BW: 350–500 g) were anesthetized with a bolus mixture of ketamine/xylazine (85/5 mg kg^{-1} , IM) then an intravenous (iv) infusion of ketamine/xylazine (40/0.5 $\text{mg kg}^{-1} \text{h}^{-1}$, to effect). The jugular vein and left carotid arteries were cannulated for test article administration and arterial blood pressure (BP) monitoring and blood collection, respectively. The body surface electrocardiogram (ECG) was measured via

subcutaneous needle electrodes to record modified lead-II ECG. After surgery, anesthetized GPs were stabilized for a minimum of 10 min before beginning baseline data collection. Solutions of 3 varying test-article concentrations suitable for administering selected doses were prepared in appropriate vehicles. Vehicle alone or test-article solutions were administered i.v. with each dose level infused over a 20-min period. Each test article and vehicle were evaluated in $\geq n = 3$ male anesthetized GPs. Blood sampling for pharmacokinetic analysis was taken at 10 and 19 min of each dose level.

2.5. *In Silico* simulation

A control population of 107 human ventricular action potential (AP) models was constructed using the O'Hara-Rudy dynamic (ORd) model (O'Hara et al., 2011) and the experimentally-calibrated population of models methodology (Britton et al., 2013; Passini et al., 2017). A description of the design of this control population of models is described in Passini et al., 2019 (Passini et al., 2019).

All simulations in this study were conducted using the Virtual Assay (v.1.3.6402014 Oxford University Innovation Ltd. Oxford, UK), a C++ based software package for *in silico* drug assays (Passini et al., 2017).

Drug effects were simulated using a simple pore-block model (Brennan et al., 2009), with IC₅₀'s acquired internally using whole-cell automated PX (PatchXpress®) and/or HTS methods for 4 ion channels: fast Na⁺ current (I_{Na}) and rapid/slow delayed rectified K⁺ current (I_{Kr}/I_{Ks}), and L-type Ca²⁺ current (I_{CaL}). *In Silico* data was generated by either using the combination of IC₅₀'s from PX (I_{Na} and I_{Kr}/I_{Ks}) and the Ca²⁺ influx fluorescence assay (I_{CaL}) or the combination of the HTS IC₅₀'s generated using MK-0499 Filter Binding Assay (I_{Kr}), the Ca²⁺ FLIPR (I_{CaL}) and the hNav1.5 FLIPR Assay.

Multiple concentrations of each compound were investigated (0, 0.03, 0.1, 0.3, 1, 3 and 10 μM) in the 107-simulated cell model. These concentrations typically cover a wide enough range that is relevant and sufficiently above (> 30-fold) the projected free clinical concentrations of the selected NCEs. Virtual cells were paced at 1 Hz for 500 beats and the last AP and Ca²⁺ transient traces of each simulation were compared with the corresponding control (500 beats at 1 Hz in the absence of drug). All AP traces were checked for repolarization and depolarization abnormalities. For cell models not displaying abnormalities, the average action potential duration at 90% repolarization (APD₉₀) and the Ca²⁺ transient duration at 90% of repolarization (CTD₉₀) were computed, along with a single cell approximation of the *in vivo* EMw, defined as the difference between Ca²⁺ transient duration at 90% (CTD₉₀) and APD₉₀, as shown in Fig. 1 (Passini et al., 2019).

2.6. Translational pharmacokinetic and pharmacodynamic (tPKPD) M5 pruned model

M5 tree is a decision tree model that allows to develop classification systems that predict or classify future observations based on a set of decision rules. It has been developed for dealing with regression task and operates on continuous numerical dependent variable (Quinlan, 1992). In general, they follow the classification and regression tree (CART) approach, but the leaf node constant value has been replaced by fitted multivariate linear regression model. One of the features of the M5 trees is automatic pruning (M5P) that allows for effective tree size reduction. For each internal node, the algorithm compares the estimated error of that node and estimated error of a subtree below the node. In the situation when the subtree does not provide added performance value of the whole tree, it is cut off. M5P trees have been widely used in multiple areas and various problems (Freitas et al., 2015). The M5P building algorithm implemented in the Waikato environment for knowledge analysis (WEKA) was used during the study. A similar approach was previously used to analyze cardiac safety of antituberculous drugs (Polak et al., 2018).

The model development was preceded by the data pre-processing.

The above described *in silico* generated data that were used as they stand, however the *in vitro* measured IC₅₀ values were re-calculated from nanomolar (nM) to micromolar (μM) and negative logarithm (pIC₅₀) was calculated. The output declared as tPKPD QTc EC₅ was recalculated to the logarithmic value (see Table 5).

The model development was based on the leave-one-out (LOO) methodology and automatic pruning. The former means that the algorithm of automatic tree building was restarted n times (where "n" – number of compounds in original learning dataset) and every time 1 compound was excluded to serve as internal validation. An identical methodology was applied to develop multiple linear regression-based models, which were further used as the comparators and point of reference for the MP5 based models. In each case linear regression-based models' performance was lower as compared against the model of choice – M5P trees.

The original input dataset consisted of 12 *in silico* computed parameters and 7 ('PX' approach) or 3 ('HT' approach) *in vitro* measured data (Table 1). The automated pruning algorithm reduced the input vectors as presented in Table 2.

3. Results

3.1. Ion Channel, *In Silico* and anesthetized CVGP assay data

A general workflow to determine the predictive capacity of the *in silico* model alone or the *in silico* model in combination with a tPKPD model to predict the CVGP QTc interval prolongation results is presented in the supplementary section. In summary, the ion channel inhibition data was generated for $n = 73$ NCEs using PX and $n = 51$ of the same set of NCEs using HTS methods (Table 3). The NCEs (all small molecules) were from various chemical classes which cover 5 therapeutic areas and over 41 different mechanisms of action. The ion channel IC₅₀'s are used as inputs for the *in silico* model which simulates the effects at varying NCE concentrations on the virtual ventricular action potentials and electromechanical window. The qualitative directional effect on the simulated APD₉₀ and EMw are reported in Table 5 along with the tPKPD predicted and the actual CVGP unbound concentrations at which we observed a 5% increase in QTc interval in the CVGP (QTc EC₅). Using the qualitative directional effects on the simulated APD₉₀ and EMw enables the determination of the predictive capacity of the *in silico* model alone to prolong the QTc interval in the CVGP (described in section 3.3). In general, compounds that prolong the QTc interval and the action potential, respectively in the CVGP and *in silico* assays, will also shorten the EMw *in silico*. NCEs that are mixed ion channel inhibitors typically do not prolong the QTc interval in the CVGP assay and do not shorten the simulated EMw, *in silico*. Also, NCEs that have hCaV1.2 IC₅₀'s which are within 2-fold of the hERG or MK-499 IC₅₀ don't typically prolong the CVGP QTc interval or simulated action potential and tend to prolong the simulated EMw.

Combining the *in silico* model results with the predicted QTc EC₅ (Table 5) from the tPKPD model enables the re-evaluation of the predictive capacity (Fig. 3C and D) of the *in silico* model results in combination with the tPKPD model to prolong the QTc interval in the anesthetized CVGP (described in section 3.4). In general, this will reclassify several compounds that were identified as false positives given it is now possible to relate the predicted QTc EC₅ to the actual concentration achieved in the anesthetized CVGP.

3.2. Probabilistic assessment of QTc prolongation in the anesthetized CVGP assay using hERG or MK-499 inhibition data alone

Confusion matrix analysis (Fig. 2) was conducted using either the PX hERG or MK-499 IC₂₀'s as compared to the CVGP QTc EC₅ concentrations for each NCE (Table 2). NCE's were qualified as "true positive" (TP) to prolong the QTc interval in the CVGP if the hERG or MK-499 IC₂₀'s was lower or within 5-fold as compared to the CVGP QTc

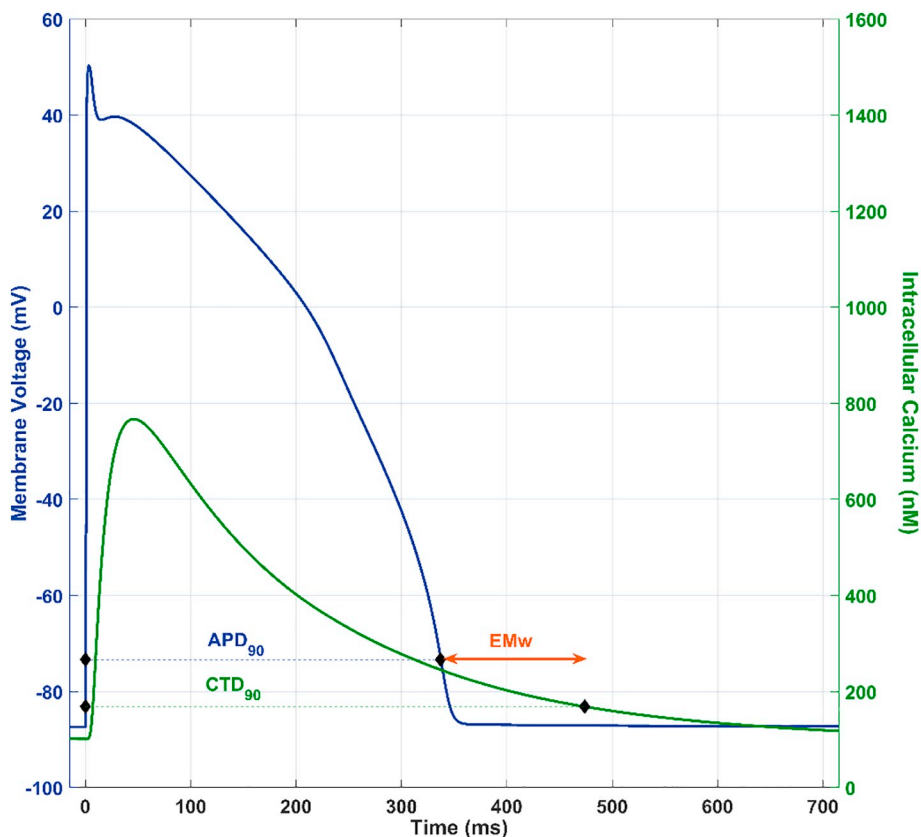


Fig. 1. *In silico* APD₉₀ and EMw. The EMw is defined here as the difference between the Ca²⁺ Transient Duration at 90% repolarization (CTD₉₀) and the action potential duration at 90% repolarization (APD₉₀).

Table 1

In vitro data used as the input information for the M5P-based model in two tested approaches PX and HTS, respectively.

Approach parameter (pIC50)	PX	HTS
High Throughput MK-499 Binding		×
High Throughput hNav1.5		×
High Throughput I _{Ca}	×	×
PatchXpress I _{Na} (hNav1.5)	×	
PatchXpress I _{Na} (hNav1.5) Hill Coefficient	×	
PatchXpress I _{Kr} (hERG)	×	
PatchXpress I _{Kr} (hERG) Hill Coefficient	×	
PatchXpress I _{Ks} (KCNQ1/ KCNE1)	×	
PatchXpress I _{Ks} (KCNQ1/ KCNE1) Hill Coefficient	×	

Table 2

Final input parameters specific for PX and HTS.

QTC	
'PX'	'HTS'
PatchXpress I _{Kr} (hERG) IC ₅₀	High Throughput MK-499 Binding IC ₅₀
PatchXpress I _{Kr} (hERG) Hill Coeff.	High Throughput hNav1.5 IC ₅₀
High Throughput I _{Ca} IC ₅₀	High Throughput I _{Ca} IC ₅₀
PatchXpress hNav1.5 IC ₅₀	Average maximum upstroke velocity (dV/dt_MAX) for all simulated cells at the 3rd highest concentration tested
Average resting membrane potential (RMP) for all simulated cells at the 4th highest concentration tested	
Average resting membrane potential (RMP) for all simulated cells at the 5th highest concentration tested	
Average peak voltage (V _{peak}) in simulated cells at 5th highest concentration tested	
Average Ca ²⁺ -transient duration at 50% (CTD ₅₀) of the initial base value for all simulated cells at the 2nd highest concentration tested	
Average action potential duration at 50% (APD ₅₀) repolarization for all simulated cells at the third highest concentration tested	

EC₅. If the PX hERG or MK-499 IC₂₀'s was > 5-fold than the CVGP QTc EC₅, they were qualified as “false negative” (FN). NCE's were qualified as “true negative” (TN) if their hERG or MK-499 IC₂₀ was larger than the highest free concentration achieved in the CVGP for which QTc interval prolongation was not observed. In these instances, the CVGP QTc EC₅ was not defined and was listed as being greater than the highest free plasma concentration tested in Table 4. NCE's were qualified as “false positive” (FP) if the PX hERG or MK-499 IC₂₀'s was lower than the highest concentration achieved in the CVGP without QTc interval prolongation.

Using this set of rules, it was determined that specificity is similar using either PX or MK-499 binding data to predict QTc interval prolongation in the CVGP. However, the rate of false negatives using PX

Table 3
Ion channel inhibition data from the PX and HTS platforms.

NCE	PX hERG IC ₅₀ (μM)	PX hNav1.5 IC ₅₀ (μM)	PX I _{Ks} IC ₅₀ (μM)	HTS hCav1.2 IC ₅₀ (μM)	HTS MK-499 IC ₅₀ (μM)	HTS hNav1.5 IC ₅₀ (μM)
1	0.01	8.3	ND	3.25	0.01	43
2	0.95	9.4	270	ND	NA	NA
3	26.5	ND	ND	ND	26	NA
4	1	0.6	100	ND	NA	NA
5	0.007	6.7	ND	3	1.1	5.3
6	2.6	11	5.9	0.1	NA	NA
7	42	ND	ND	ND	NA	NA
8	12	68	5.7	7.4	3.1	12.4
9	36	15	79	16.2	9.9	0.5
10	18	14	ND	ND	NA	NA
11	8.2	48	100	12.6	24.7	ND
12	27	68	150	ND	NA	NA
13	0.86	100	ND	5.1	0.3	3.5
14	27	75	ND	13.3	10.8	4.7
15	55	ND	ND	ND	53	ND
16	25	ND	ND	ND	NA	NA
17	15	43	21	16.9	32.6	39
18	21	94	ND	13.4	34.3	12.9
19	40	45	6	27	2.2	ND
20	27	ND	ND	79	49	ND
21	11	19	13	ND	NA	NA
22	26	43	150	35	41.6	15.2
23	31	45	ND	ND	NA	NA
24	6.4	100	ND	11	47	14
25	8.1	36	ND	ND	NA	NA
26	0.58	11	44	ND	NA	NA
27	50	ND	ND	ND	38	ND
28	14	ND	ND	21.4	34.9	ND
29	40	50	ND	2.8	46	136
30	11	ND	ND	ND	32.3	ND
31	22	ND	ND	ND	33	ND
32	23	36	ND	ND	NA	NA
33	48	4.1	38	19	5.7	29.4
34	22	55	ND	7	41.9	23.4
35	26	ND	ND	21.5	31.2	ND
36	4.5	16	63	ND	NA	NA
37	29	ND	ND	115	39	29
38	12	42	ND	6.9	6.4	10.9
39	10	94	ND	27.9	10.4	19.2
40	21	19	ND	43	56.5	ND
41	8.5	38	ND	ND	NA	NA
42	26	4	15	16.4	11.1	12.7
43	35	ND	83	18.6	50	ND
44	47	21	29	13.8	18.4	28.8
45	58	ND	ND	ND	28	ND
46	5.3	ND	ND	107	10.9	94
47	12	36	115	18.4	19.8	15.1
48	56	68	48	28.7	47.2	88
49	44	60	ND	9.1	ND	83
50	82	53	ND	ND	NA	NA
51	0.95	45	ND	17.5	3.6	ND
52	19	150	83	ND	6.3	31.8
53	5.4	ND	ND	300	NA	NA
54	2.5	60.9	15	3.12	NA	NA
55	2.1	23	300	0.785	1.7	5.6
56	1	70	106	3	16.1	ND
57	4.8	0.94	300	ND	26.7	ND
58	0.14	638	31	2.3	0.42	2.8
59	0.33	7.5	95	10	NA	NA
60	25	ND	ND	26	NA	NA
61	1.8	17	14	4.9	3	ND
62	4.3	15	3.7	0.47	3.8	31
63	9.1	90	300	0.195	3.8	7.5
64	1.5	300	300	4.1	ND	ND
65	1.1	12	60	1.3	3.6	ND
66	2.2	300	300	1.75	3.3	20.3
67	0.14	ND	ND	ND	NA	NA
68	4	ND	ND	19.04	22.9	19.5
69	2	ND	ND	20.4	ND	ND
70	5	53.3	300	ND	19.5	ND
71	11	13.5	ND	3.087	NA	NA

Table 3 (continued)

NCE	PX hERG IC ₅₀ (μM)	PX hNav1.5 IC ₅₀ (μM)	PX I _{Ks} IC ₅₀ (μM)	HTS hCav1.2 IC ₅₀ (μM)	HTS MK-499 IC ₅₀ (μM)	HTS hNav1.5 IC ₅₀ (μM)
72	83	35	ND	ND	NA	NA
73	3.3	6.9	13.6	1.251	NA	NA

ND: An IC₅₀ was not determined, no meaningful inhibition (< 10% inhibition) was observed at the highest tested concentration (30 μM), NA: No data is available: the NCE was not tested.

hERG inhibition data was lower as compared to when MK-499 binding data was used which resulted in higher sensitivity with the PX data.

3.3. Probabilistic assessment of QTc interval prolongation in the anesthetized CVGP assay using the qualitative outcome of in silico simulated APD prolongation and EMw shortening

Effects on simulated APD₉₀ and EMw using either HTS (n = 51 NCEs) or PX ion channel data (n = 73 NCEs) was computed at various drug concentrations (6 concentrations per NCE) and their qualitative results were compared to the CVGP QTc EC₅ interval effect. Confusion matrix analysis was conducted to assess the concordance of the *in silico* results using PX (Fig. 3A) or HTS data (Fig. 3B) to predict QTc interval prolongation in the CVGP. NCEs were qualified as “positive” *in silico* to prolong the QTc interval in the CVGP when both the APD₉₀ prolonged and the EMw shortened from baseline over the range of tested concentrations. However, if the simulated APD₉₀ did not prolong and/or the EMw did not shorten (< 5% change over the range of concentrations tested), the NCE was considered “negative” to prolong the QTc interval in the CVGP assay. In the CVGP, a compound was considered “positive” if it prolonged the QTc interval over the range of tested concentrations and a CVGP QTc EC₅ was defined. If there was no QTc prolongation in the CVGP the NCE was defined as “negative” *in vivo* and the CVGP QTc EC₅ was listed in Table 5 to be greater than the highest free plasma concentration tested in the CVGP. As such, a TP NCE was identified if both the simulated APD₉₀ prolonged and the simulated EMw shortened and a CVGP QTc EC₅ was defined. A TN NCE was defined if no CVGP QTc EC₅ was identified and the APD₉₀ shortened or the EMw prolonged. The confusion matrix results for each individual NCE are presented in Table 5 and applied in Fig. 3. Higher sensitivity to predict QTc interval prolongation in the CVGP is achieved when using the *in silico* model outcomes generated with PX ion channel data as compared to when using HTS ion channel data. Specificity is similar when using PX or MK-499 data as inputs for the *in silico* model.

3.4. Probabilistic assessment of QTc interval prolongation in the anesthetized CVGP assay when adjusted with the tPKPD model results

The concentration at which a CVGP QTc EC₅ would occur was evaluated using either the HTS or PX ion channel data in a M5-pruned tPKPD model. The correlation between the projected free plasma concentration that caused a 5% prolongation in QTc interval with the HTS or PX tPKPD models and the actual plasma concentration that caused a 5% increase in QTc interval in the CVGP were plotted for all the NCEs that were qualified as positive in section 3.3 (Fig. 4A and B). In general results are within 5-fold of the unity line.

Positive NCEs (TP and FP) were further analyzed using the tPKPD results and confusion matrices are presented in Fig. 3B and D for HTS and PX data, respectively. However, all negative NCEs identified using the *in silico* model were considered negative and, as such, not further analyzed using the tPKPD model. All the TP compounds identified in section 3.3 stayed positive if the tPKPD model predicted QTc EC₅ concentrations within 5-fold of the actual CVGP QTc EC₅. In addition, if

Table 4
Confusion matrix results comparing the PX hERG IC₂₀ or HTS MK-499 binding IC₂₀ to the CVGP QTc EC₅.

Compound	Guinea pig QTc EC ₅ (μM) ^a	PX hERG IC ₂₀ (μM)	PX hERG IC ₂₀ Confusion matrix result PX	HTS MK-499 IC ₂₀ (μM)	HTS MK-499 Confusion matrix result HTS
1	0.07	0.004	TP	0.003	TP
2	1.2	0.2	TP	NA	NA
3	1.8	12	FN	9.2	FN
4	1.6	0.4	TP	NA	NA
5	0.02	0.0028	TP	0.3	FN
6	> 3	1.04	FP	NA	NA
7	15	15.2	TP	NA	NA
8	> 0.7	4.8	TN	0.8	TN
9	> 2	12	TN	1.9	FP
10	1.6	8.1	FN	NA	NA
11	> 5	2.6	FP	8.2	TN
12	> 8.7	7.5	FP	> 30	TN
13	1	0.2	TP	0.1	TP
14	> 5.4	12	TN	3.5	FP
15	> 20	21	TN	19.2	FP
16	10	8.7	TP	NA	NA
17	> 5	5.5	FP	12.4	TN
18	> 0.385	8.4	TN	12.6	TN
19	> 0.05	16	TN	0.82	FP
20	> 7.7	9.2	TN	18.5	TN
21	> 0.1	4.3	TN	NA	NA
22	> 0.89	10.1	TN	15.4	TN
23	5	17	FN	ND	NA
24	7.2	1.5	TP	15.2	TP
25	1.2	6.5	FN	ND	NA
26	1	0.2	TP	NA	NA
27	> 4.5	21	TN	14.2	TN
28	> 4.6	4.2	FP	11.1	TN
29	> 0.14	12	TN	16.2	TN
30	4	3.5	TP	8.2	TP
31	> 2	8	TN	12.5	TN
32	6	7.5	TP	NA	NA
33	> 0.1	16	TN	1.6	TN
34	> 16	7.2	FP	14.8	FP
35	> 45.8	8.4	FP	12.48	FP
36	3.5	1.5	TP	NA	NA
37	> 2.5	10.8	TN	14.2	TN
38	> 60	3.5	FP	2.4	FP
39	0.9	3.5	TP	4.1	TP
40	1.4	7.6	FN	18.5	FN
41	> 4.4	2.5	FP	NA	NA
42	> 0.27	8.3	TN	3.5	TN
43	> 5.5	12	TN	18.2	TN
44	> 1.98	16	TN	6.5	TN
45	44	19.4	TP	10.5	TP
46	0.988	2.5	TP	3.8	TP
47	> 0.2	3.6	TN	6.4	TN
48	> 4.7	20.6	TN	16.2	TN
49	> 0.3	15.4	TN	6.8	TN
50	> 31	33.3	TN	NA	NA
51	0.3	0.2	TP	1.1	TP
52	2.8	5.4	TP	2.1	TP
53	0.4	2.2	TP	NA	NA
54	> 0.4	0.8	TN	NA	NA
55	> 1	0.56	FP	0.68	FP
56	1.8	0.2	TP	6.44	TP
57	2	1.4	TP	10.1	FN
58	0.23	0.056	TP	0.168	TP
59	> 3.3	0.132	FP	NA	NA
60	19.9	8.2	TP	NA	NA
61	0.1	0.34	TP	0.8	FN
62	> 0.2	3.4	TN	1.1	TN
63	> 0.4	5.2	TN	1.3	TN
64	> 0.07	0.8	TN	ND	TN
65	1	0.33	TP	1.1	TP
66	> 3.4	0.56	FP	0.9	FP
67	0.3	0.05	TP	NA	NA
68	3	1.1	TP	8.2	TP
69	0.5	0.6	TP	NA	NA

Table 4 (continued)

Compound	Guinea pig QTc EC ₅ (μM) ^a	PX hERG IC ₂₀ (μM)	PX hERG IC ₂₀ Confusion matrix result PX	HTS MK-499 IC ₂₀ (μM)	HTS MK-499 Confusion matrix result HTS
70	1.2	1.7	TP	6.5	FN
71	> 2.3	6.2	TN	NA	NA
72	> 5.4	28.4	TN	NA	NA
73	> 0.8	1.4	TN	NA	NA

TP: True Positive, TN: True Negative, FP: False Positive, FN: False Negative, ND: An IC₅₀ was not determined, no meaningful inhibition was observed at the highest tested concentration (30 μM), NA: No data is available: the NCE was not tested.

^a The listed concentrations are free plasma concentrations.

other factors can influence it. Factors that predispose to QT prolongation and higher risk of torsades de pointes in the clinic include age, female sex, left ventricular hypertrophy, ischemia, slow heart rate, and electrolyte abnormalities including hypokalemia and hypomagnesemia (Ahnve, 1985; Khan, 2002; Locati et al., 1998; Makkar et al., 1993). Given the goal of the current study was to predict the QTc interval outcome in an early development *in vivo* model, adjustments were not made for these additional factors in the *in silico* model. The focus was rather on the main ion currents that underly the ventricular AP and how the simulated models' AP relate to the QTc interval. In addition, the specific interaction of the NCE with the ion channels such as kinetics and drug dissociation or reassociation was beyond the scope of this study. Only the drug's ion channel IC_{50s} were used as inputs to evaluate resource sparing method at this early stage of development.

Our results support that the *in silico* assay used in combination with tPKPD modeling can have qualitative and quantitative agreement with this commonly used preclinical safety pharmacology assay in early drug development. The accuracy of the *in silico* simulations to predict QTc interval prolongation in the CVGP assay is superior to the ones obtained using solely ion channel data from the PX hERG or MK-499 binding assays. In fact, the negative predictive value (NPV) when using solely PX hERG inhibition data (85%, Fig. 2A) in absence of *in silico* modeling is lower as compared to using mixed ion channel inhibition data from PX (hERG, I_{Ks}, hNav1.5 and hCav1.2) *in silico* (100%, Fig. 3A). This is in part due to the O'Hara Rudy (ORD) model's (O'Hara et al., 2011) increased sensitivity to hERG block (Mirams et al., 2014) which will identify ADP₉₀ and/or QTc interval prolongation at lower concentrations. As such, NCEs that are identified as FN when using hERG data alone are correctly identified as TP using the *in silico* model. However, the NPV when using HTS ion channel data (MK-499 binding IC_{50s}) is similar (80%, Fig. 3B) to the MK-499 data alone (85%, see Fig. 2B). This is likely due to lower affinity in the MK-499 binding results as compared to the PX assay results for most of the FN (compound 3, 5, 40, 57, 61 and 70). Differences in affinity between PX and HTS methods may be related to the PX assay which can reveal a functional block that is associated with potential allosteric modulation that does not displace a ligand at the ion channel pore in a standard binding assay. In addition, binding to isolated membranes may differ from intact cells (*i.e.*, access to binding site or different ionic conditions in both assays) and affinities may vary for different states of the channel.

In contrast, the positive predictive value (PPV) for PX hERG (70%), HTS MK-499 (72%), PX *In silico* (75%) and HTS *in silico* (67%) to predict QTc interval prolongation in the anesthetized CVGP assay were similar. The FP NCEs using hERG and MK-499 data alone are generally the result of not integrating mixed ion channel inhibition data from other channels (hCav1.2, hNav1.5 and I_{Ks}). As such, many of these compounds are correctly classified as TN when using *in silico* simulation (NCE# 6, 11, 17, 28, 34, 35, 55, 66). The *in silico* simulation is able to distinguish between drugs which purely affect I_{Kr} and those with a

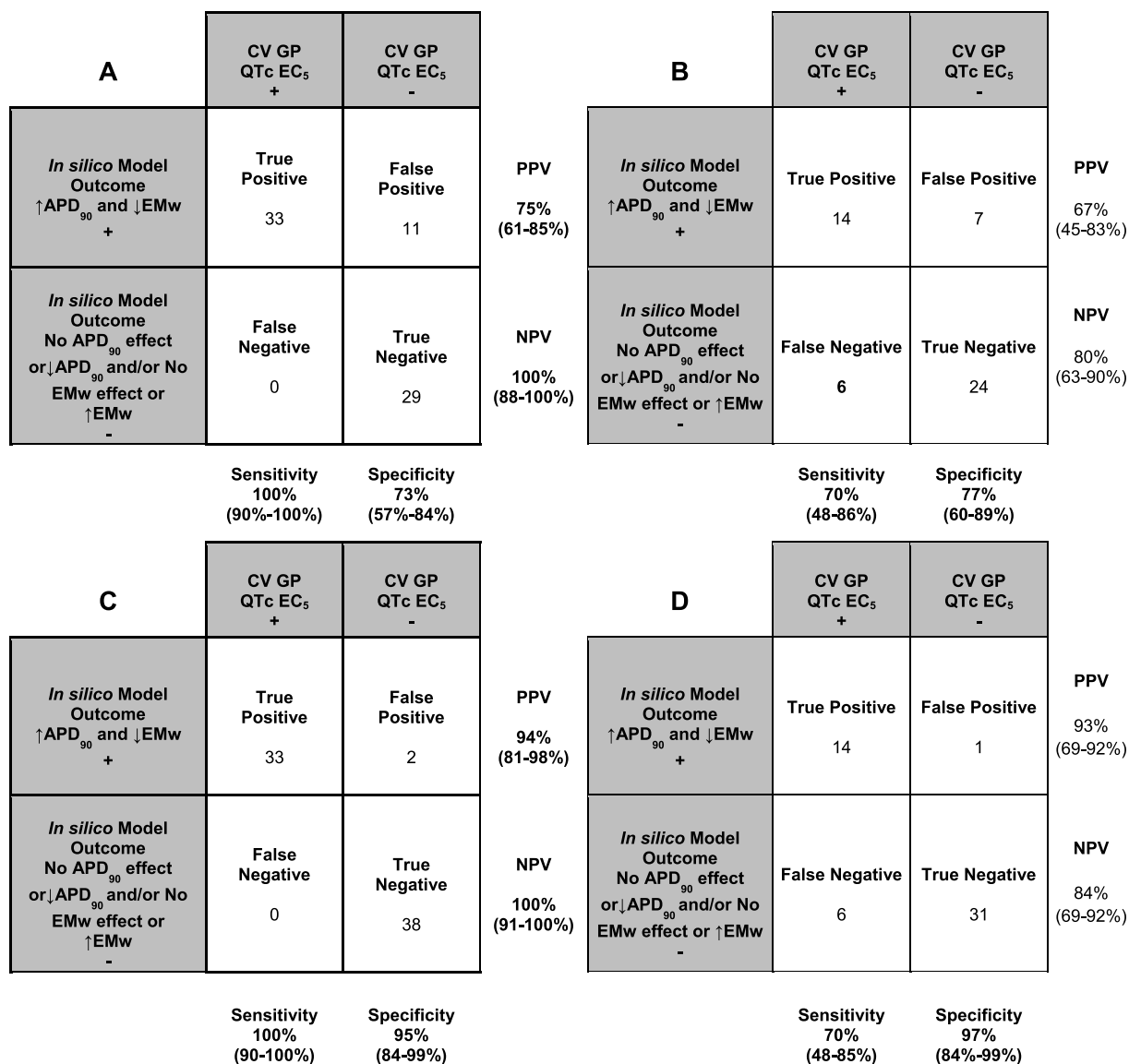


Fig. 3. Matrix results (with 95% confidence intervals indicated) using the *in silico* model endpoints (APD₉₀ and EMw) relative to the CVGP Qtc EC₅ using *in vitro* ion channel data obtained from PX (A) or HTS (B) and matrix results when adjusted with tPKPD model projected Qtc EC₅ using PX (C) or HTS (D) ion channel data. PPV: Positive predictive value, NPV: Negative predictive value.

multi-channel action which modify Ca²⁺ dynamics given the ability of the model to predict the effect on the EMw which has been shown to be more sensitive to drug-induced changes in Ca²⁺ transient (Passini et al., 2019). *In vivo*, the EMw is a measure of the temporal dispersion of the duration of the electrical and mechanical systole which is related to the duration of repolarization on the ECG and to the levels of intracellular Ca²⁺ in a measure of contractility. Typically, potent I_{Kr} blockers will have very little effect on simulated Ca²⁺ transient and will prolong the simulated APD₉₀ and the *in vivo* Qtc interval as opposed to those NCEs displaying hCav1.2 block, that do not shorten the EMw when cardiac adverse events are less likely to occur. *In vivo*, shortening of the EMw has been presented as an effective biomarker of proarrhythmia in several preclinical experimental studies (Guns et al., 2012a; Guns et al., 2012b; Morissette et al., 2016; van der Linde et al., 2010). A negative EMw, formerly referred to in the clinic as inversed QT/QS2 ratio or “QT > QS2 Syndrome”, occurs if either LV-contraction duration shortens or if the QT-interval prolongs (or a combination of both). It was shown that in the healthy myocardium, the duration of electrical systole (QT) is shorter than that of the electromechanical systole (Second heart sound; QS₂ in the clinic), which it closely parallels

throughout the range of resting heart rate (HR) (Boudoulas et al., 1982). More recently, ter Bekke et al. (2015) observed that patients with genotype-positive long QT syndrome exhibit EMw inversion and it is most pronounced in patients with documented arrhythmic events. Given the sensitivity of the EMw to detect mixed ion channel inhibition, this parameter was used to increase the sensitivity of the *in silico* model to predict Qtc interval prolongation in the CVGP. However, the simulated EMw was not used, in this instance, to predict arrhythmic risk.

The remaining FP compounds identified when using the qualitative *in silico* model results (Fig. 3A and B) are a different set of NCEs from using ion channel alone (Fig. 2A and B) and are generally due to the high sensitivity of the ORd model to hERG inhibition as well as to the ability of testing high concentrations that may not be achievable and/or tolerated *in vivo*. As a result, the tPKPD model becomes useful in determining if the concentration at which we observe Qtc interval prolongation is relevant. This model allows for the prediction of the concentration at which we observe meaningful Qtc interval prolongation in the anesthetized CVGP assay. When the tPKPD model predicts that the concentration at which we observe Qtc interval prolongation is greater than the highest concentration achieved in the CVGP with no

Table 5
Confusion matrix results using qualitative outcomes from *in silico* simulated endpoints or when adjusted with tPKPD QTc EC₅ projected concentrations.^a

Compound	CVGP QTc EC ₅ (μM) ^a	Data generated using PX ion channel data				Data generated using HTS ion channel data					
		<i>In Silico</i> APD ₉₀ directional effect	<i>In Silico</i> EMw directional effect	Confusion matrix result using only <i>in silico</i> results	tPKPD QTc EC ₅ (μM) ^a	Confusion matrix result adjusted with tPKPD results	<i>In Silico</i> APD ₉₀ directional effect	<i>In Silico</i> EMw directional effect	Confusion matrix result	tPKPD QTc EC ₅ (μM) ^a	Confusion matrix result adjusted for tPKPD results
1	0.07	↑	↓	TP	0.03	TP	↑	↓	TP	0.08	TP
2	1.2	↑	↓	TP	2.4	TP	NA	NA	NA	NA	NA
3	1.8	↑	↓	TP	1.9	TP	↑	↓	TP	4.8	TP
4	1.6	↑	↓	TP	1.5	TP	NA	NA	NA	NA	NA
5	0.02	↑	↑↓	TP	0.02	TP	↑	↓	TP	0.21	FN
6	> 3	↑	↑	TN	2.9	TN	NA	NA	NA	NA	NA
7	12	↑	↓	TP	15	TP	NA	NA	NA	NA	NA
8	> 0.7	↑	↑	TN	1.3	TN	↑	↑	TN	0.5	TN
9	> 2	↑	↑	TN	1.9	TN	↑	↑	TN	5.7	TN
10	1.6	↑	↓	TP	6.01	TP	NA	NA	NA	NA	NA
11	> 5	↑	↑	TN	3.1	TN	↑	↑	TN	0.3	TN
12	> 8.7	↑	↓	FP	9.2	TN	↑	↑	TN	468	TN
13	1	↑	↓	TP	0.4	TP	0.03	0.03	TP	0.1	TP
14	> 5.4	↑	↑	TN	10.9	TN	↑	↑	TN	2.5	TN
15	> 20	↑	↓	FP	28	TN	↑	↓	FP	32	TN
16	10	↑	↓	TP	19.9	TP	NA	NA	NA	NA	NA
17	> 5	↑	↑	TN	3.4	TN	↑	↑	TN	3	TN
18	> 0.385	↑	↑	TN	17	TN	↑	↑	TN	4.3	TN
19	> 0.05	↑	↑	TN	2	TN	↑	↓	FP	0.08	TN
20	> 7.7	↑	↓	FP	6.1	FP	↑	↓	FP	1.1	FP
21	> 0.1	↑	↓	FP	5.2	TN	NA	NA	NA	NA	NA
22	> 0.89	↑	↑	TN	2.2	TN	↑	↑	TN	6.9	TN
23	5	↑	↓	TP	9.1	TP	NA	NA	NA	NA	NA
24	7.2	↑	↓↑	TP	1	TP	↑	↑	FN	4.9	FN
25	1.2	↑	↓	TP	5.1	TP	NA	NA	NA	NA	NA
26	1	↑	↓	TP	1.6	TP	NA	NA	NA	NA	NA
27	> 4.5	↑	↓	FP	4.7	TN	↑	↓	FP	6.4	TN
28	> 4.6	↑	↑	TN	1.4	TN	↑	↑	TN	0.5	TN
29	> 0.14	↓	↑	TN	12	TN	↓	↓	TN	1.2	TN
30	4	↑	↓	TP	14.1	TP	↑	↓	TP	5.6	TP
31	> 2	↑	↓	FP	3.6	TN	↑	↓	FP	5.7	TN
32	6	↑	↓	TP	9.6	TP	NA	NA	NA	NA	NA
33	> 0.1	↑	↑	TN	4.2	TN	↑	↓	FP	0.9	TN
34	> 16	↑	↑	TN	18	TN	↑	↑	TN	3.1	TN
35	> 45.8	↑	↑	TN	5.6	TN	↑	↑	TN	0.5	TN
36	3.5	↑	↓	TP	3.6	TP	NA	NA	NA	NA	NA
37	> 2.5	↑	↓	FP	3	TN	↑	↓	FP	8.5	TN
38	> 60	↑	↑	TN	1.2	TN	↑	↑	TN	0.9	TN
39	0.9	↑	↓	TP	1.2	TP	↑	↓	TP	2	TP
40	1.4	↑	↓	TP	2	TP	↑	↑	FN	0.9	FN
41	> 4.4	↑	↓	FP	5.2	TN	NA	NA	NA	NA	NA
42	> 0.27	↑	↑	TN	1.9	TN	↑	↑	TN	1.9	TN
43	> 5.5	↑	↑	TN	2.1	TN	↑	↑	TN	0.6	TN
44	> 1.98	↑	↑	TN	2.4	TN	↑	↑	TN	2	TN
45	44	↑	↓	TP	29	TP	↑	↓	TP	5	TP
46	0.988	↑	↓	TP	1	TP	↑	↓	TP	2	TP
47	> 0.2	↑	↑	TN	1.3	TN	↑	↑	TN	3	TN
48	> 4.7	↑	↑	TN	2.7	TN	↑	↑	TN	1	TN
49	> 0.3	↑	↑	TN	4.2	TN	↓	↑	TN	147	TN
50	> 31	↑	↑	TN	134	TN	NA	NA	NA	NA	NA
51	0.3	↑	↓	TP	0.5	TP	↑	↓	TP	0.07	TP
52	2.8	↑	↓	TP	5.2	TP	↑	↓	TP	12.5	TP
53	0.4	↑	↓	TP	1	TP	NA	NA	NA	NA	NA
54	> 0.4	↑	↑	TN	0.6	TN	NA	NA	NA	NA	NA
55	> 1	↑	↑	TN	0.4	TN	↑	↑	TN	0.16	TN
56	1.8	↑	↓	TP	0.5	TP	↑	↑	FN	0.12	FN
57	2	↑	↓	TP	1	TP	↑	↓	TP	4.1	TP
58	0.23	↑	↓	TP	0.2	TP	↑	↓	TP	0.12	TP
59	> 3.3	↑	↓	FP	0.2	FP	NA	NA	NA	NA	NA
60	19.9	↑	↓	TP	10	TP	NA	NA	NA	NA	NA
61	0.1	↑	↓	TP	0.5	TP	↑	↑	FN	0.04	FN
62	> 0.2	↑	↑	TN	0.4	TN	↑	↑	TN	0.12	TN
63	> 0.4	↓↑	↑	TN	0.4	TN	↑	↑	TN	0.12	TN
64	> 0.07	↑	↓	FP	0.5	TN	↓	↑	TN	18.9	TN
65	1	↑	↓	TP	0.2	TP	↑	↓	TP	0.1	TP
66	> 3.4	↑	↑	TN	0.5	TN	↑	↑	TN	0.3	TN
67	0.3	↑	↓	TP	0.4	TP	NA	NA	NA	NA	NA
68	3	↑	↓	TP	0.7	TP	↑	↑	FN	3.1	FN
69	0.5	↑	↓	TP	0.6	TP	↓	↑	FN	37	FN

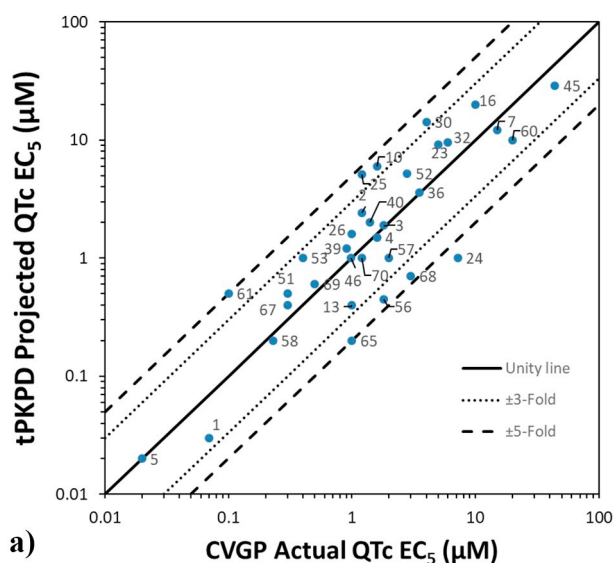
(continued on next page)

Table 5 (continued)

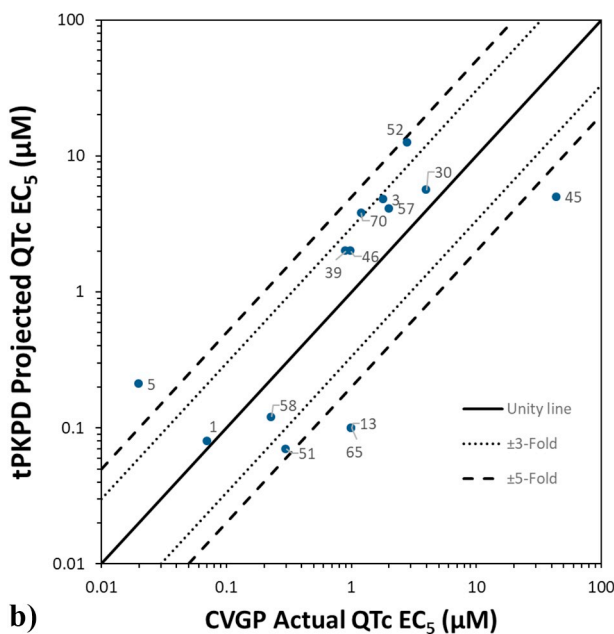
Compound	CVGP QTc EC ₅ (μM) ^a	Data generated using PX ion channel data					Data generated using HTS ion channel data				
		<i>In Silico</i> APD ₉₀ directional effect	<i>In Silico</i> EMw directional effect	Confusion matrix result using only <i>in silico</i> results	tPKPD QTc EC ₅ (μM) ^a	Confusion matrix result adjusted with tPKPD results	<i>In Silico</i> APD ₉₀ directional effect	<i>In Silico</i> EMw directional effect	Confusion matrix result	tPKPD QTc EC ₅ (μM) ^a	Confusion matrix result adjusted for tPKPD results
70	1.2	↑	↓	TP	1	TP	↑	↓	TP	3.8	TP
71	> 2.3	↑	↑	TN	4.2	TN	NA	NA	NA	NA	NA
72	> 5.4	↑	↓	FP	34	TN	NA	NA	NA	NA	NA
73	> 0.8	↑	↑	TN	1	TN	NA	NA	NA	NA	NA

↑: Increase at tested concentrations, ↓ decrease at tested concentrations, ↓↑ decrease followed by an increase at higher concentrations, TP: True Positive, TN: True Negative, FP: False Positive, FN: False Negative, ND: IC₅₀ was not determined, no meaningful inhibition (< 10% inhibition) was observed at the highest tested concentration (30 μM), NA: No data is available, the NCE was not tested.

^a The listed concentrations are free plasma concentrations.



a)



b)

Fig. 4. Translational Pharmacokinetic/Pharmacodynamic (tPKPD) results: A) tPKPD projected QTc EC₅ as compared to actual CVGP QTc EC₅ when using PX ion channel data. B) tPKPD projected QTc EC₅ as compared to the actual CVGP QTc EC₅ when using high throughput (HTS) ion channel data. Data points are labeled with their NCE number found in Tables 3-5.

QTc interval prolongation, the compound is correctly reclassified as TN. As a result, when the *in silico* model is used in combination with the tPKPD model, the PPV increases to 94% and 93% using PX or HTS ion channel data, respectively.

The remaining FP NCEs (NCE #20 and #59 for PX and #20 for HTS) after applying the tPKPD model are likely due to another activity that contributes to a modulation of calcium cycling which could counterbalance the effects on AP repolarization and QTc interval prolongation. For example, a mechanism that reduces intracellular Ca²⁺ such as by decreasing cAMP could counteract QTc interval prolongation and have a protective effect. As a result, it is important to understand the putative mechanism of action or potential off-target activity of NCEs to consider other mechanisms that may influence the overall repolarization outcome. Since these additional mechanisms are not standard *in silico* inputs, the model may not always accurately predict the final *in vivo* outcome. In these circumstances, it is important that NCEs continue to be tested *in vivo* prior to further progression into later development. In addition, other potential risk factors associated with QTc interval prolongation such as hypothermia (Rai et al., 2014), hypokalemia (Weiss et al., 2017), glucose levels/hypoglycemia (Sertbas et al., 2017), metabolites active on hERG, accumulation of test article in the myocardium, and/or inhibition of the translocation/trafficking of the hERG channel to the membrane (Eckhardt et al., 2005) will not be evaluated *in silico* unless this is known *a priori* and is integrated into the model. Moreover, additional cardiovascular information provided from an *in vivo* assay such as hemodynamic assessment, changes in cardiac contractility, effect on autonomic nervous system (ortho- & parasympathetic) balance and/or cardio-renal baroreflexes, and effects on cardiac conduction are not currently predicted from single cell *in silico* assays, as the ones considered in this study. However, novel frameworks to run multiscale simulations are currently being developed (Lopez-Perez et al., 2019; Vigmond et al., 2009), also including computer model of human contraction (Fritz et al., 2014; Land et al., 2017), which will allow to compute additional *in silico* biomarkers.

The anesthetized CVGP assay has previously been compared to results in the non-rodent (dog and monkeys) and the clinic (QTc) to assess its usefulness in early derisking (Morissette et al., 2013). High levels of sensitivity (75–100%), and specificity (100%) was observed. The overall accuracy of the anesthetized CVGP assay was very high (92–100%), given the outcome of the non-rodent telemetry models were well predicted by the CVGP. In addition, there was a robust correlation between the CVGP and non-rodent free plasma concentrations (≤ 10-fold difference) that produced comparable changes in QTc interval in non-rodent and the clinic. Consequently, it could be argued that *in silico* results in combination with tPKPD modeling could also be used to predict meaningful free plasma concentrations that would prolong QTc intervals in the non-rodent GLP assays and FIH clinical studies.

5. Conclusions

This study demonstrated that the combination of an *in silico* cardiac electrophysiological model and a tPKPD model is highly predictive, sensitive (low rate of FN NCEs), and specific (low rate of FP NCEs) for predicting QTc interval prolongation in a commonly used *in vivo* model, the anesthetized CVGP. Simulated APD₉₀ and EMw changes observed *in silico* are qualitatively predictive of QTc interval changes in the anesthetized CVGP. Using tPKPD modeling to predict threshold QTc prolongation concentrations in the CVGP correctly re-classified NCE's and increased the overall positive predictive value (PPV). Ultimately, these comparative approaches demonstrated the predictive value of an *in silico*, tPKPD model to determine *in vivo* QTc prolongation. Consequently, we should consider the use of such approaches early in the NCE discovery research process to increase throughput, query a broader range of compounds to better assess QTc risk liabilities in an early *in vivo* derisking model, and potentially reduce animal, costs & resource intensive *in vivo* studies. Finally, it would be consistent with the "3Rs" paradigm for animal research and should enable a faster advancement of NCEs into preclinical and clinical development.

Declaration of Competing Interest

The authors declare no conflicts of interest.

Appendix A. Supplementary data

Supplementary data to this article can be found online at <https://doi.org/10.1016/j.taap.2020.114883>.

References

- Ahnve, S., 1985. QT interval prolongation in acute myocardial infarction. *Eur. Heart J.* 6 (Suppl D), 85–95.
- Balasubramanian, B., Imredy, J.P., Kim, D., Penniman, J., Lagrutta, A., Salata, J.J., 2009. Optimization of Ca(v)1.2 screening with an automated planar patch clamp platform. *J. Pharmacol. Toxicol. Methods* 59, 62–72.
- Beattie, K.A., Luscombe, C., Williams, G., Munoz-Muriedas, J., Gavaghan, D.J., Cui, Y., Mirams, G.R., 2013. Evaluation of an *in silico* cardiac safety assay: using ion channel screening data to predict QT interval changes in the rabbit ventricular wedge. *J. Pharmacol. Toxicol. Methods* 68, 88–96.
- Boudoulas, H., Sohn, Y.H., O'Neill, W., Brown, R., Weissler, A.M., 1982. The QT greater than QS2 syndrome: a new mortality risk indicator in coronary artery disease. *Am. J. Cardiol.* 50, 1229–1235.
- Brennan, T., Fink, M., Rodriguez, B., 2009. Multiscale modelling of drug-induced effects on cardiac electrophysiological activity. *Eur. J. Pharm. Sci.* 36, 62–77.
- Britton, O.J., Bueno-Orovio, A., Van Ammel, K., Lu, H.R., Towart, R., Gallacher, D.J., Rodriguez, B., 2013. Experimentally calibrated population of models predicts and explains intersubject variability in cardiac cellular electrophysiology. *Proc. Natl. Acad. Sci. U. S. A.* 110, E2098–E2105.
- Colatsky, T., Fermini, B., Gintant, G., Pierson, J.B., Sager, P., Sekino, Y., Strauss, D.G., Stockbridge, N., 2016. The comprehensive *In Vitro* Proarrhythmia Assay (CiPA) initiative - update on progress. *J. Pharmacol. Toxicol. Methods* 81, 15–20.
- Davies, M.R., Mistry, H.B., Hussein, L., Pollard, C.E., Valentin, J.P., Swinton, J., Abi-Gerges, N., 2012. An *in silico* canine cardiac midmyocardial action potential duration model as a tool for early drug safety assessment. *Am. J. Phys. Heart Circ. Phys.* 302, H1466–H1480.
- Di Diego, J.M., Sicouri, S., Myles, R.C., Burton, F.L., Smith, G.L., Antzelevitch, C., 2013. Optical and electrical recordings from isolated coronary-perfused ventricular wedge preparations. *J. Mol. Cell. Cardiol.* 54, 53–64.
- Eckhardt, L.L., Rajamani, S., January, C.T., 2005. Protein trafficking abnormalities: a new mechanism in drug-induced long QT syndrome. *Br. J. Pharmacol.* 145, 3–4.
- Fermini, B., Fossa, A.A., 2003. The impact of drug-induced QT interval prolongation on drug discovery and development. *Nat. Rev. Drug Discov.* 2, 439–447.
- Fermini, B., Jurkiewicz, N.K., Jow, B., Guinasso Jr., P.J., Baskin, E.P., Lynch Jr., J.J., Salata, J.J., 1995. Use-dependent effects of the class III antiarrhythmic agent NE-10064 (azimilide) on cardiac repolarization: block of delayed rectifier potassium and L-type calcium currents. *J. Cardiovasc. Pharmacol.* 26, 259–271.
- Freitas, A.A., Limbu, K., Ghafourian, T., 2015. Predicting volume of distribution with decision tree-based regression methods using predicted tissue:plasma partition coefficients. *J. Cheminform* 7, 6.
- Fritz, T., Wieners, C., Seemann, G., Steen, H., Dossel, O., 2014. Simulation of the contraction of the ventricles in a human heart model including atria and pericardium. *Biomech. Model. Mechanobiol.* 13, 627–641.
- Guns, P.J., Johnson, D.M., Van Op den Bosch, J., Weltens, E., Lissens, J., 2012a. The electro-mechanical window in anaesthetized Guinea pigs: a new marker in screening for torsades de pointes risk. *Br. J. Pharmacol.* 166, 689–701.
- Guns, P.J., Johnson, D.M., Weltens, E., Lissens, J., 2012b. Negative electro-mechanical windows are required for drug-induced Torsades de pointes in the anesthetized Guinea pig. *J. Pharmacol. Toxicol. Methods* 66, 125–134.
- Heist, E.K., Ruskin, J.N., 2010. Drug-induced arrhythmia. *Circulation* 122, 1426–1435.
- Khan, I.A., 2002. Clinical and therapeutic aspects of congenital and acquired long QT syndrome. *Am. J. Med.* 112, 58–66.
- Land, S., Park-Holohan, S.J., Smith, N.P., dos Remedios, C.G., Kentish, J.C., Niederer, S.A., 2017. A model of cardiac contraction based on novel measurements of tension development in human cardiomyocytes. *J. Mol. Cell. Cardiol.* 106, 68–83.
- Locati, E.H., Zareba, W., Moss, A.J., Schwartz, P.J., Vincent, G.M., Lehmann, M.H., Towbin, J.A., Priori, S.G., Napolitano, C., Robinson, J.L., Andrews, M., Timothy, K., Hall, W.J., 1998. Age- and sex-related differences in clinical manifestations in patients with congenital long-QT syndrome: findings from the international LQTS registry. *Circulation* 97, 2237–2244.
- Lopez-Perez, A., Sebastian, R., Izquierdo, M., Ruiz, R., Bishop, M., Ferrero, J.M., 2019. Personalized cardiac computational models: from clinical data to simulation of infarct-related ventricular tachycardia. *Front. Physiol.* 10, 580.
- Makkar, R.R., Fromm, B.S., Steinman, R.T., Meissner, M.D., Lehmann, M.H., 1993. Female gender as a risk factor for torsades de pointes associated with cardiovascular drugs. *JAMA* 270, 2590–2597.
- Mirams, G.R., Davies, M.R., Brough, S.J., Bridgland-Taylor, M.H., Cui, Y., Gavaghan, D.J., Abi-Gerges, N., 2014. Prediction of thorough QT study results using action potential simulations based on ion channel screens. *J. Pharmacol. Toxicol. Methods* 70, 246–254.
- Morissette, P., Nishida, M., Trepakova, E., Imredy, J., Lagrutta, A., Chaves, A., Hoagland, K., Hoe, C.M., Zrada, M.M., Travis, J.J., Zingaro, G.J., Gerenser, P., Friedrichs, G., Salata, J.J., 2013. The anesthetized Guinea pig: an effective early cardiovascular derisking and lead optimization model. *J. Pharmacol. Toxicol. Methods* 68, 137–149.
- Morissette, P., Regan, C., Fitzgerald, K., Gerenser, P., Travis, J., Wang, S., Fanelli, P., Sannajust, F., 2016. Shortening of the electromechanical window in the ketamine/xyzazine-anesthetized Guinea pig model to assess pro-arrhythmic risk in early drug development. *J. Pharmacol. Toxicol. Methods* 81, 171–182.
- Muskiewicz, A., Britton, O.J., Gemmill, P., Passini, E., Sanchez, C., Zhou, X., Carusi, A., Quinn, T.A., Burrage, K., Bueno-Orovio, A., Rodriguez, B., 2016. Variability in cardiac electrophysiology: using experimentally-calibrated populations of models to move beyond the single virtual physiological human paradigm. *Prog. Biophys. Mol. Biol.* 120, 115–127.
- Nemec, J., Kim, J.J., Salama, G., 2016. The link between abnormal calcium handling and electrical instability in acquired long QT syndrome - does calcium precipitate arrhythmic storms? *Prog. Biophys. Mol. Biol.* 120, 210–221.
- O'Hara, T., Virag, L., Varro, A., Rudy, Y., 2011. Simulation of the undiseased human cardiac ventricular action potential: model formulation and experimental validation. *PLoS Comput. Biol.* 7, e1002061.
- Passini, E., Britton, O.J., Lu, H.R., Rohrbacher, J., Hermans, A.N., Gallacher, D.J., Greig, R.J.H., Bueno-Orovio, A., Rodriguez, B., 2017. Human *in silico* drug trials demonstrate higher accuracy than animal models in predicting clinical pro-arrhythmic cardiotoxicity. *Front. Physiol.* 8.
- Passini, E., Trovato, C., Morissette, P., Sannajust, F., Bueno-Orovio, A., Rodriguez, B., 2019. Drug-induced shortening of the electromechanical window is an effective biomarker for *in silico* prediction of clinical risk of arrhythmias. *Br. J. Pharmacol.* 176, 3819–3833.
- Penniman, J.R., Kim, D.C., Salata, J.J., Imredy, J.P., 2010. Assessing use-dependent inhibition of the cardiac Na⁺ current (I_{Na}) in the PatchXpress automated patch clamp. *J. Pharmacol. Toxicol. Methods* 62, 107–118.
- Picard, S., Goineau, S., Rouet, R., 2006. The action potential of the Purkinje fiber: an *in vitro* model for evaluation of the proarrhythmic potential of cardiac and noncardiac drugs. *Curr. Protoc. Pharmacol.* <https://doi.org/10.1002/0471141755.ph1103s33>. Chapter 11, Unit11.13.
- Polak, S., Romero, K., Berg, A., Patel, N., Jamei, M., Hermann, D., Hanna, D., 2018. Quantitative approach for cardiac risk assessment and interpretation in tuberculosis drug development. *J. Pharmacokinetic. Pharmacodyn.* 45, 457–467.
- Quinlan, R.J., 1992. Learning with continuous classes. In: 5th Australian Joint Conference on Artificial Intelligence, Singapore.
- Rai, M., Cronin, E.M., Kluger, J., LaSala, A.F., 2014. Hypothermia and left ventricular dysfunction: the role of electric changes. *J. Am. Soc. Echocardiogr.* 27, 680.
- Salvi, V., Karnad, D.R., Panicker, G.K., Kothari, S., 2010. Update on the evaluation of a new drug for effects on cardiac repolarization in humans: issues in early drug development. *Br. J. Pharmacol.* 159, 34–48.
- Schmitz, S., Henke, J., Tacke, S., Guth, B., 2016. Successful implantation of an abdominal aortic blood pressure transducer and radio-telemetry transmitter in Guinea pigs - Anesthesia, analgesic management and surgical methods, and their influence on hemodynamic parameters and body temperature. *J. Pharmacol. Toxicol. Methods* 80, 9–18.
- Sertbas, Y., Ozdemir, A., Sertbas, M., Dayan, A., Sancak, S., Uyan, C., 2017. The effect of glucose variability on QTc duration and dispersion in patients with type 2 diabetes mellitus. *Pak. J. Med. Sci.* 33, 22–26.
- ter Bekke, R.M., Haugaa, K.H., van den Wijngaard, A., Bos, J.M., Ackerman, M.J., Edwardsen, T., Volders, P.G., 2015. Electromechanical window negativity in genotyped long-QT syndrome patients: relation to arrhythmia risk. *Eur. Heart J.* 36, 179–186.
- Trepakova, E.S., Malik, M.G., Imredy, J.P., Penniman, J.R., Dech, S.J., Salata, J.J., 2007. Application of PatchXpress planar patch clamp technology to the screening of new drug candidates for cardiac KCNQ1/KCNE1 (I_{Ks}) activity. *Assay Drug Dev. Technol.* 5 (5), 617–627.

- Valentin, J.-P., Hoffmann, P., De Clerck, F., Hammond, T.G., Hondeghem, L., 2004. Review of the predictive value of the Langendorff heart model (Screenit system) in assessing the proarrhythmic potential of drugs. *J. Pharmacol. Toxicol. Methods* 49, 171–181.
- van der Linde, H.J., Van Deuren, B., Somers, Y., Loenders, B., Towart, R., Gallacher, D.J., 2010. The electro-mechanical window: a risk marker for torsade de pointes in a canine model of drug induced arrhythmias. *Br. J. Pharmacol.* 161, 1444–1454.
- Vigmond, E., Vadakkumpadan, F., Gurev, V., Arevalo, H., Deo, M., Plank, G., Trayanova, N., 2009. Towards predictive modelling of the electrophysiology of the heart. *Exp. Physiol.* 94, 563–577.
- Weiss, J.N., Qu, Z., Shivkumar, K., 2017. Electrophysiology of hypokalemia and hyperkalemia. *Circ. Arrhythm. Electrophysiol.* 10.
- Xia, M., Imredy, J.P., Koblan, K.S., Bennett, P., Connolly, T.M., 2004. State-dependent inhibition of L-type calcium channels: cell-based assay in high-throughput format. *Anal. Biochem.* 327, 74–81.
- Zeng, H., Penniman Trepakova ES, Malik MG, Dech SJ, Balasubramanian B, Salata JJ, J.R., Kinose, F., Kim, D., Trepakova, E.S., Malik, M.G., Dech, S.J., Balasubramanian, B., Salata, J.J., 2008. Improved throughput of PatchXpress hERG assay using intracellular potassium fluoride. *Assay Drug Dev. Technol.* 6 (2), 235–241.